Atmos. Chem. Phys., 11, 11631–11645, 2011
www.atmos-chem-phys.net/11/11631/2011/
doi:10.5194/acp-11-11631-2011

Atmospheric Chemistry and Physics

Using a mobile laboratory to characterize the distribution and transport of sulfur dioxide in and around Beijing

M. Wang[1,*], T. Zhu[1], J. P. Zhang[2], Q. H. Zhang[2], W. W. Lin[1,*], Y. Li[3], and Z. F. Wang[4]

[1]State Key Laboratory of Environmental Simulation and Pollution Control, College of Environmental Sciences and Engineering, Peking University, Beijing, 100871, China
[2]Department of Atmospheric and Oceanic Sciences, School of Physics, Peking University, Beijing, 100871, China
[3]Chinese Academy of Meteorological Science, Beijing, 100081, China
[4]Nansen-Zhu International Research Centre, Institute of Atmospheric Physics, Chinese Academy of Sciences, Beijing, 100871, China
[*]present address: Institute for Risk Assessment Sciences, Utrecht University, The Netherlands

Received: 30 March 2011 – Published in Atmos. Chem. Phys. Discuss.: 6 June 2011
Revised: 4 November 2011 – Accepted: 11 November 2011 – Published: 22 November 2011

Abstract. Megacities are places with intensive human activity and energy consumption. To reduce air pollution, many megacities have relocated energy supplies and polluted industries to their outer regions. However, regional transport then becomes an important source of air pollution in megacities. To improve air quality before and during the 2008 Beijing Olympics, a wide range of control strategies were implemented, including the relocation of polluting industries. High sulfur dioxide (SO_2) concentrations were occasionally observed during this period. Potential sources from southern regions of Beijing were indicated by backward trajectories model and urban/rural stationary measurements, but direct evidence was lacking. Here we used a mobile laboratory to characterize the spatial distribution and regional transport of SO_2 to Beijing during the Campaign for Air Quality Research in Beijing and the Surrounding Region (CAREBEIJING)-2008. Among the five days chosen for the case studies during the Olympic air pollution control period, four had high SO_2 concentrations (6, 20 August and 3, 4 September 2008) while one had low SO_2 concentration (11 September 2008). The average values of SO_2 during the low SO_2 concentration day were 3.9 ppb, much lower than during the high concentration days (7.8 ppb). This result implied an impact by regional transport from outside Beijing. During these days, we captured transport events of SO_2 from areas south of Beijing, with a clear decrease in SO_2 concentrations southeast of the 6th to 4th Ring Roads around Beijing and along the 140 km highway from Tianjin to Beijing. The influx of SO_2 through the 4th to 6th Ring Roads ranged from 2.1 to 4.6 kg s^{-1} on 4 September and 0.2 to 1.6 kg s^{-1} on 20 August 2008. The differences of influx in days were due to the variations of emission changes, transport directions and dilutions. Locally emitted SO_2 from a source located along Jingshi Highway outside the southwest section of the 5th Ring Road of Beijing was identified using wind field data generated by the Weather Research and Forecasting model and the measured particle size distribution, with an estimated flux of 0.1 kg s^{-1} to Beijing. Estimated uncertainties for SO_2 influx were approximately 31 %.

Correspondence to: T. Zhu
(tzhu@pku.edu.cn)

1 Introduction

Sulfur dioxide (SO_2) is one of the most important precursors of secondary aerosols in the atmosphere. It is responsible for severe air pollution, leading to degraded visibility, changes in the radiation budget, and acid rain (Wang et al., 2008; Zhang et al., 2004a; Ramanathan and Crutzen, 2003). In addition, SO_2 is harmful to human health (Brunekreef and Holgate, 2002) and may cause increased respiratory diseases, reduced pulmonary function, low birth weight, and mortality (Xu et al., 1998).

Rapid economic development, industrialization, and urbanization have occurred within and around the megacity of Beijing, increasing demands for fossil fuel consumption (Ohara et al., 2007), which is the main source of SO_2.

In 2008, the annual average energy consumption levels in Beijing, Tianjin, and the surrounding provinces of Heibei, Shanxi, and Shandong were 63.4 (Beijing Statistical Yearbook, 2009), 53.6 (Tianjin Statistical Yearbook, 2009), 242.2 (Hebei Statistical Yearbook, 2009), 268.8 (Shanxi Statistical Yearbook, 2009), and 125.1 (Shandong Statistical Yearbook, 2009) million tons of standard coal, respectively. To improve air quality and maintain clean air throughout the 2008 Beijing Olympic Games, the Beijing municipal government implemented comprehensive long- and short-term air pollution control measures. The measures included moving heavy polluters out of the city, using low sulfur coal and high standard fuel (e.g. Euro IV), reducing the number of on-road vehicles, and freezing construction activities before and during the Olympic Games. While significant decreases in SO_2 were reported during the Olympics (Wang et al., 2009a, b; Qin et al., 2009), periods with relatively high SO_2 concentrations occasionally occurred during the Olympic period, suggesting an important role of the regional transport of SO_2 emitted outside Beijing.

Previous studies have reported that both local emission and regional transport sources contribute to SO_2 in Beijing (Zhang et al., 2004b; Xu et al., 2004; Sun et al., 2004). Rural/urban stationary (Liu et al., 2008; Guo et al., 2010) and tower observations (Sun et al., 2009) in Beijing have revealed that high wind speeds from southern areas might play a vital role in the increase of SO_2 concentrations in Beijing. An et al. (2007) used the Community Multiscale Air Quality (CMAQ) model to simulate the regional transport of SO_2 and its flux pathway during a heavy pollution episode. They estimated that the southeast and southern areas of Beijing contributed 26 % and 18 % of SO_2 to the city. However, due to uncertainties in the SO_2 emission inventory outside Beijing, it is difficult to model the dispersion and transport of SO_2 accurately on small scales (Matsui et al., 2009). Thus, direct evidence from spatial distribution measurements is required.

Aircraft-based measurement with fast response instruments is a suitable approach to both studying the spatial distribution and quantifying the regional transport flux of SO_2 (Wang et al., 2006; Matvev et al., 2002; Beryrich et al., 1998). In northern China (where Beijing is located), research on SO_2 transport using aircraft measurements has focused on large-scale processes (Li et al., 2010; Ma et al., 2010; Ding et al., 2009) in the upper boundary layer or in the free troposphere. Given the high cost of aircraft measurement and difficulties in obtaining navigation approval, on-road measurement from mobile laboratories is an optimal method for ground-based spatial distribution measurement. On-road measurement platforms have been specifically designed and used for three types of applications: investigation of emission factors of individual vehicles by chasing studies (Canagaratna et al., 2004; Herndon et al., 2005), examination of the temporal-spatial variations in air pollutants for exposure assessment (Bukowiecki et al., 2002; Weijers et al., 2004), and quantification of local emissions and regional transport flux (Johansson et al., 2009; Rivera et al., 2009). Johansson et al. (2008) and Li et al. (2009) calculated SO_2 fluxes from local emissions in Beijing using mobile-based mini-differential optical absorption spectroscopy (DOAS) around the 5th Ring Road of Beijing. However, these calculations were only based on column concentrations of SO_2. There is hence a lack of information on the ground level transport and concentrations of other air pollutants.

Here we used an on-road mobile laboratory to measure the spatial distribution of SO_2 concentrations and identify transport processes in the southern part of Beijing. These observations were part of the Campaign for Air Quality Research in Beijing and the Surrounding Region-2008 (CAREBEIJIING)-2008. The flux of SO_2 from both local emission and regional transport was estimated using wind field data from the Weather Research and Forecasting (WRF) model version 3.1.1.

2 Methodology

2.1 Mobile laboratory and driving routes

Details of the setup and performance of the instruments installed in the mobile laboratory were described in our previous paper (Wang et al., 2009a). Briefly, a diesel vehicle (IVECO Turin V) was selected as the mobile platform. To minimize the loss of particles in the sampling inlet, an isokinetics inlet system was designed to enhance the sampling efficiency. The instruments onboard provided data on the concentrations of gaseous pollutants (NO-NO_2-NO_x, SO_2, CO, CO_2, O_3) (ECOTECH, Australia), black carbon (MAAP, THERMO, USA), particle surface area (Nanoparticle surface area monitor, TSI, USA), particle size distribution (SMPS, DMA 3080 and CPC 3550, TSI, USA), and volatile organic compounds (VOCs; PTR-MS, IONICON, Austria). In this paper only the data of SO_2 and SMPS were used (Table 2). The time resolutions of SO_2 and SMPS data were 10 s and 2 min, respectively. Additional instruments included a Global Positioning System (GPS) and meteorological parameters (temperature, humidity, and pressure). The driving speed was $60\pm5\,\mathrm{km\,h^{-1}}$.

To characterize the spatial distribution of SO_2 and to investigate the regional transport progress of SO_2 to Beijing, routes were specially designed at local scale around the south area of Beijing, and at regional scale between Beijing and Tianjin megacities (Fig. 1). The details of routes and monitoring information are listed in Table 1. Five days were chosen for the measurements, and in general four days (6, 20 August and 3, 4 September 2008) showed high SO_2 concentrations and one day showed low SO_2 concentration (11 September 2008). We first selected routes 1 and 2 along the southeast of the Ring Roads to map the SO_2 spatial distribution within the city of Beijing. The Ring Roads cover a wide area from the urban area to the city center and thus it

Table 1. Mobile measurement dates and route types.

Cruise Route	Starting date time (LT*)	Ending date time (LT)	Route type
Route 1	20 Aug 2008 (7:58)	20 Aug 2008 (12:50)	Southeast 2th to 6th Ring RD
Route 2	4 Sep 2008 (14:13)	4 Sep 2008 (18:22)	Southeast 4th to 6th Ring RD
Route 3	3 Sep 2008 (10:05)	3 Sep 2008 (15:13)	Beijing to Tianjin
Route 4	11 Sep 2008 (10:09)	11 Sep 2008 (14:37)	Beijing to Tianjin
Route 5	6 Aug 2008 (12:00)	6 Aug 2008 (14:50)	Southwest area outside Beijing

* LT: local time.

Table 2. Instrumentation performed in this study.

Station name	Instruments	Measurement species
Mobile Laboratory	SO_2 analyzer(Ecotech 9850A, Austrilia) (10 s) scanning mobility particle sizer (SMPS) (3080, TSI Inc.) (2 min)	SO_2 Size distribution (size 14.1–667 nm)
PKU station	SO_2 analyzer(Ecotech 9850B, Austrilia) (1h) Mete One(1∼3 h)	SO_2, Wind speed, wind direction
YuFa station	SO_2 analyzer(Ecotech 9850B, Austrilia) (1h) Mete One(1∼3 h)	SO_2 Wind speed, wind direction
YongLeDian station	SO_2 analyzer(Ecotech 9850B, Austrilia) (1h) Mete One(1∼3 h)	SO_2 Wind speed, wind direction
CAMS stations	Mete One(1∼3 h)	Wind speed, wind direction

is preferable to investigate the transport of SO_2 at the local scale. Because of the limited battery power of the instruments installed on the platform, observations in the mornings and afternoons were conducted on different days. To illustrate the spatial distribution and transport of SO_2 between two megacities (Beijing and Tianjin), we selected a newly built highway (Jingjintang II) between the two cities. The highway was far from industrialized areas, and because it was newly built, it had few cars driving on it during the Olympics. Thus the anthropogenic contribution from vehicular and industrial emissions was low, and the air pollutant levels were comparable to those of background air (Wang et al., 2009a). This unique feature was favorable for studying the air mass transport.

Continuous measurements were also conducted along the southwest of the 5th Ring Road and part of the 6th Ring Road in the southern area, where high-density industry is located, as shown in Fig. 1b (blue line). The characteristics of the SO_2 distribution and its local and regional emission sources surrounding the southwest of Beijing have been reported previously (Wang et al., 2009a). Here we added wind field and particle size distribution data for a better understanding the distribution and emission sources of SO_2.

2.2 Ground-based meteorological and SO_2 measurements

Concentrations of SO_2 were simultaneously measured at three intensive monitoring stations before, during, and after the Olympics air pollution control period. The PKU station was in an urban station located at Peking University, Beijing (39.99° N, 116.31° E); YuFa (YF, 39.51° N, 116.31° E) and YongLeDian (YLD, 39.75° N, 116.73° E) were rural stations representing the regional background. They were located approximately 50 km to the south and southeast of Beijing, respectively. In addition, 11 meteorological stations (blue stars in Fig. 1) of the Chinese Academy of Meteorological Sciences (CAMS) were selected for meteorological data analysis. Table 2 shows measurement parameters and instruments at each station.

To ensure that data between different stations were comparable, the SO_2 analyzers (Ecotech, 9850B, Australia) in all the stations were automatically calibrated between 0:00 and 1:00 every day using the same certified calibration standard (50 ppb, accuracy 3 %, diluted with N_2, Beijing Huayuan Gas Chemical Industry Co., Ltd.). Calibration at five different concentrations (0 %, 20 %, 40 %, and 80 % of the detection range) was performed each time. Meanwhile, calibrations of the SO_2 analyzer on the mobile laboratory were conducted before and after each sampling trip using similar procedures as at the stations. Intercomparison of SO_2 concentrations between the mobile laboratory and PKU station

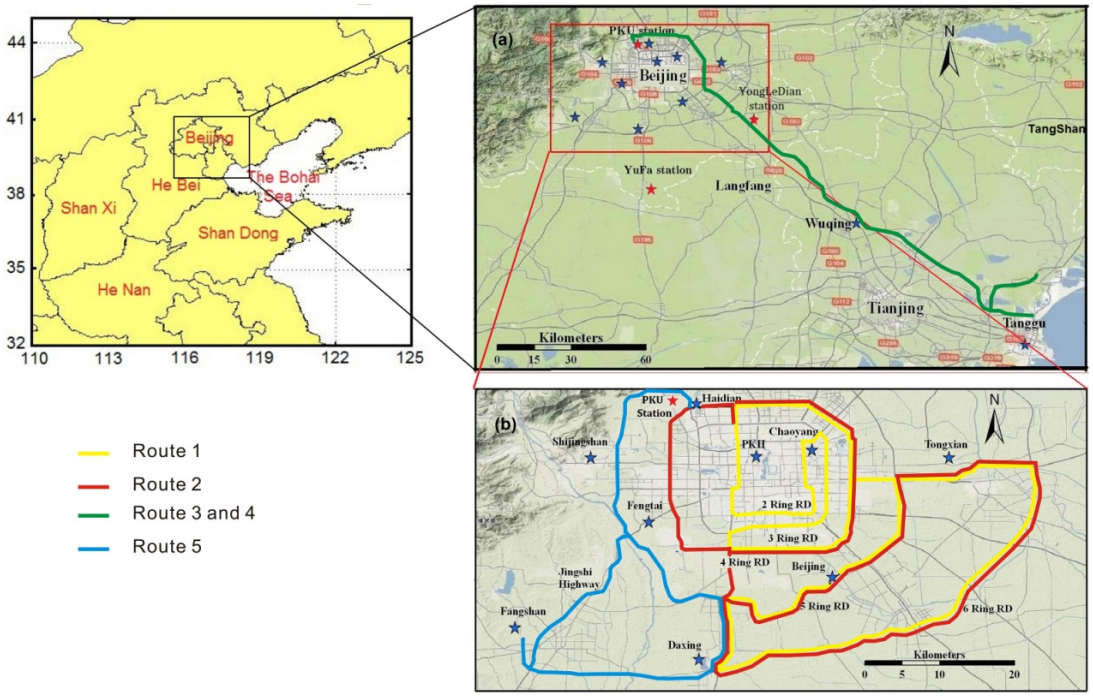

Fig. 1. Maps of the mobile monitoring areas in CAREBeijing-2008. The green track in **(a)** shows route 3 and 4 in Table 1. The red, yellow and blue tracks in **(b)** show the route 1, 2 and route 5 respectively. The red stars on the maps represent the stationary sites on SO_2 measurements and the blue stars show the CAMS meteorological stations.

was also performed. The difference between the SO_2 concentrations was within 15 %, with a correlation coefficient of 0.82 (Wang et al., 2009a).

2.3 Wind field

2.3.1 Lagrangian trajectory simulation

The Hybrid Single Particle Lagrangian Integrated Trajectory model (HYSPLIT, version 4.9), developed by the US National Oceanic and Atmospheric Administration (NOAA) Air Resources Laboratory (ARL), was used to calculate the forward and backward trajectories of plumes from or to the stations in Beijing (Draxler and Rolph, 2003). Backward trajectories were computed once every 6 h for 24 h (1 day) at a selected height of 10 m above ground level for 45 days from 1 August to 15 September, 2008 and were grouped by cluster analysis of the model. A Global Data Assimilation System (GDAS) archive meteorological database was chosen to run the trajectory model, which had $1° \times 1°$ horizontal resolution. The horizontal resolution of the model is $1° \times 1°$, which is enough to distinguish the original regions of the air masses in our study.

2.3.2 Weather Research and Forecasting (WRF) simulation

Direct measurements of wind speed and wind direction from the mobile lab during driving may lead to large deviations in the estimation of pollutant fluxes (Johansson, 2009). Here we used the WRF model version 3.1.1 to conduct mesoscale meteorological simulations for high-resolution wind fields and planetary boundary layer height (PBL) during the measurement periods. The WRF modeling system is a next-generation mesoscale numerical weather forecast and simulation system that includes the Advanced Research dynamics solver. A detailed description of the WRF model can be found on the WRF web-site http://www.wrf-model.org/index.php, as well as in our supplementary information (SI).

Here the horizontal resolution of the model was $1\,km \times 1\,km$. Four domains were used for the WRF calculation (Fig. S1). The averaged concentrations of SO_2 were calculated based on each grid unit (1×1 km in Fig. 5a, b, 2×2 km in Fig. 5c, d). The bottom level reaching 18–20 m above the surface was selected for meteorological analysis. The WRF model can simulate backward trajectories with high spatial resolution, however, to identify the main original locations of the air masses during the measurement period and classify them into regions, it is not necessary to use WRF model for such high resolution tracks as this may take a much longer time than using the Hysplit model.

Comparing the WRF modeling results with the observations from meteorological stations involved in each domain during the measurement periods, we found close agreement in the wind directions, with Pearson $R = 0.83$. The wind speed had a relatively low correlation coefficient ($R = 0.66$) (Fig. S2). This could be attributed to the complicated land use in Beijing in which the local turbulences were not only influenced by the accuracy of the measured data in the meteorological stations (near the ground level where high buildings surround) but also challenge the predictive power of the model. However, given that most of the routes were located in rural areas, we therefore used just the rural sites to calculate the correlation between model and measurements (Fig. S2), and found the correlation coefficient increased significantly both for the wind speed ($R = 0.83$) and wind direction ($R = 0.89$)

The WRF model applied the newly updated land use initialized from MODIS and contains high densities of the wind fields in the vertical level (10 layers in 1000m) and horizontal plane (1 by 1 km). These improvements of the model lead us to believe that the model is able to produce a reliable spatial distribution of the wind field.

Hourly averaged WRF-predicted PBL were compared with the temporal variations of aerosol extinction coefficient retrieved from Lidar measurements (Figs. S3, S4). We selected three days (6, 20 August and 11 September, 2008) with clear sky, well mixed convective condition; the measurement during these days provided sufficiently variable distributions of extinction coefficients. Figures S3 and S4 show that the model- calculated PBL was generally in agreement with the top boundary of the extinction coefficients during the measurement period, even though difference remained. This could be the major source of the flux uncertainty.

2.4 Assessment of the regional influx of SO_2

Quantitative assessment of SO_2 flux has been well established by the design of specified routes encircling target sources (Wang et al., 2006; Rivera et al., 2009; Johansson et al., 2008; Shaiganfar et al., 2011) or crossing frontiers perpendicular to the horizontal wind direction (Beryrich et al., 1998; Matvev et al., 2002). In this study, we carefully designed sector-routes on 20 August (route 1) and 4 September (route 2), so that the mobile tracks would likely traverse the wind direction. To calculate the transport flux outside Beijing, a simple formula based on the above measurement approach with the wind vector towards Beijing was used (White et al., 1976):

$$\mathrm{Flux}(\mathrm{kgs}^{-1}) = \sum_{i=1}^{n} C_i(\mu\mathrm{gm}^3) \cdot V_i(\mathrm{ms}^{-1}) \cdot \mathrm{Sin}\theta_i \quad (1)$$

$$\cdot H_i(m) \cdot d_i(m) \times 10^{-9}(\mathrm{kg}\mu\mathrm{g}^{-1})$$

where

Flux – the total SO_2 flux across the ring road with n $1\times1\,\mathrm{km}^2$ unit cells ($\mathrm{kg\,s^{-1}}$)

C_i – the mean concentration of SO_2 ($\mu\mathrm{g\,m^{-3}}$) in the ith grid ($1\times1\,\mathrm{km}^2$)

θ_i – the angle between wind direction and the driving route in the ith grid ($1\times1\,\mathrm{km}^2$)

V_i – wind speed ($\mathrm{m\,s^{-1}}$) in the ith grid ($1\times1\,\mathrm{km}^2$) generated by WRF output

H – mixing layer height (m) in the ith grid ($1\times1\,\mathrm{km}^2$) generated by WRF output

n – total grids ($1\times1\,\mathrm{km}^2$) of each traverse path.

d_i – the transect length (m) of the mobile route in the ith grid ($1\times1\,\mathrm{km}^2$).

The principles of the flux calculations have been mentioned in Fig. S5. To estimate fluxes based on Eq. (1), several assumptions were necessary: (1) wind speed and direction were constant during the hour (the hourly mean wind field was used), (2) the atmospheric boundary layer was stable and well-mixed during the measurement period, and the vertical distributions of SO_2 concentrations were homogenous, and (3) the wind speed is constant between emission and measurement.

3 Results and discussion

3.1 SO_2 concentration time series

Figure 2 shows the time series of SO_2 concentration from the three stations during the air pollution control period. In general, SO_2 concentrations were low during the Olympic air pollution control period (8 to 24 August 2008) at all stations, with average values of 5.8 ppb in the city and 3.2 ppb in rural areas. However, there were three periods with high SO_2 concentration at all stations: 3–10 August, 19–30 August, and 2–8 September (Fig. 2). During these periods, SO_2 concentrations varied dramatically, with diurnal peak levels higher than 15 ppb. During the 2008 Beijing Olympics period, most of the SO_2 emission sources were strictly controlled within and around Beijing (Wang et al., 2009a) and the reduction of SO_2 was estimated to be about 47 % compared with the days before the Olympics; therefore, we assumed that local emission within Beijing city was not a major source of the increase in SO_2. Hence regional transport of SO_2 under specific meteorological conditions, e.g., wind speed and wind direction, assumed to be the major cause.

To further investigate the possible source(s) of the observed SO_2, 24-h back trajectories were used to examine the air masses arriving in Beijing during the measurement

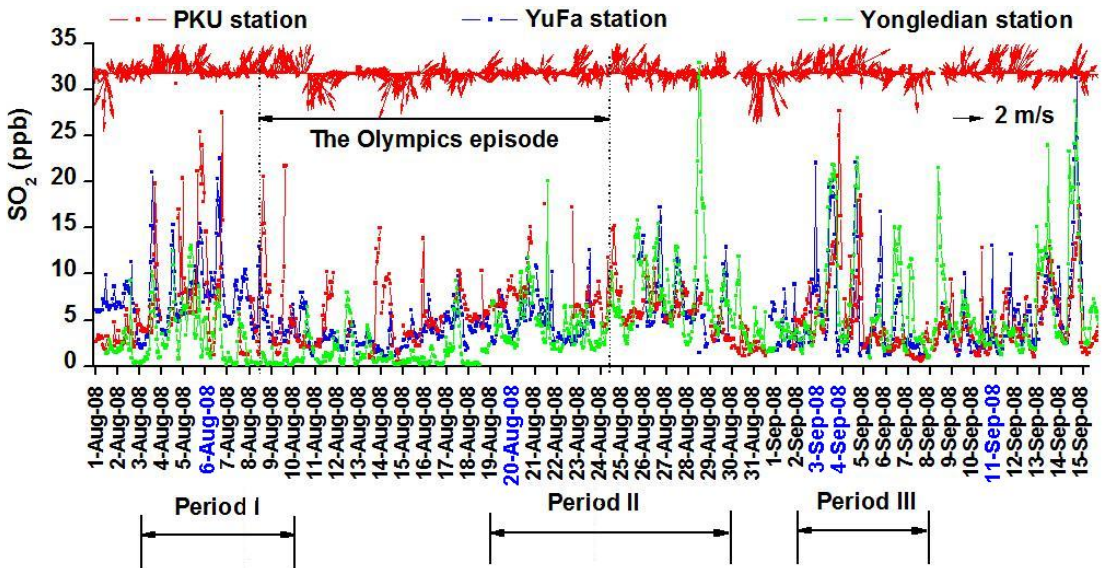

Fig. 2. Temporal variations of SO_2 concentrations at PKU, YuFa and YongLeDian stations from 1 August to 15 September 2008. The reduction of SO_2 during the Olympic period was approximately 47 % comparing with the days before the Olympics. The mobile sampling days are marked in blue color. The red arrows show the wind vectors at PKU station. Period I, II and III show the potential SO_2 pollution periods with increase trends between 3–10 August, 19–30 August and 2–8 September.

period. A total of 184 trajectories (4 per day) were generated from the center of Beijing and then classified into four groups by cluster analysis. This revealed four typical source regions. Figure 3 shows the three clusters that arose from regional transport outside Beijing. The first group of trajectories (blue) originated from the Bohai Sea in the southeast of China and then moved over the Tianjin and Tangshan areas. The second group (green) was southerly from inland China, passing over Henan and Hebei provinces. The third group (red) was from the northwest of Inner Mongolia and the northeast regions of China. The last group (not shown here) travelled locally around Beijing city. Among the 184 trajectories, clusters 1, 2, 3, and 4 accounted for 22 %, 28 %, 26 %, and 24 % of the total trajectory, respectively. The 24-h trajectories of clusters 1 and 2 were short, due to the slow wind speed, and thus SO_2 might have accumulated in Beijing. In contrast, the long trajectories of cluster 3 indicated strong winds from the northern area, which brought clean air and were favorable to air dispersion. Figure 4 shows the mean SO_2 concentration in Beijing for each trajectory cluster. As expected, high SO_2 concentrations were observed on the same days as the trajectory clusters 1 and 2. The average SO_2 concentrations ranged from 5.7 to 7.8 ppb. Trajectory clusters 3 and 4 were associated with low SO_2 concentrations, which ranged from 3.9 to 4.8 ppb, respectively.

Apparently, regional transport played an important role in increasing SO_2 concentrations in Beijing. To further investigate the SO_2 transport into Beijing, we used three mobile laboratory measurements to provide spatial distributions of SO_2 and to quantify its regional influx into Beijing.

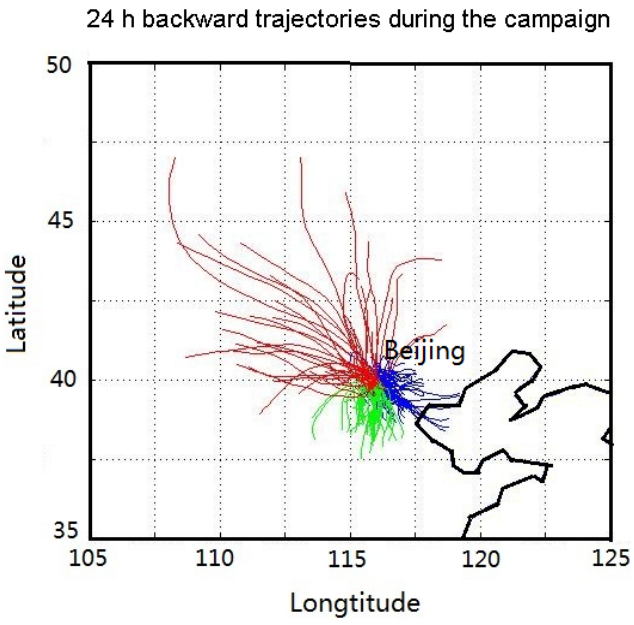

Fig. 3. 24-h Air mass backward trajectories at 10m above ground level at Beijing from 1 August to 15 September 2008. The red, green and blue trajectories show the plumes from north, south and southeast regions.

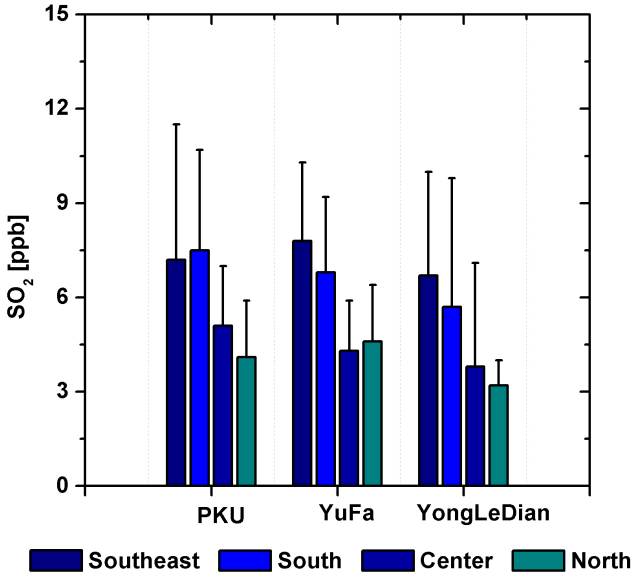

Fig. 4. The average concentrations of SO_2 measured at PKU, YuFa and YongLeDian sites subdivided on the basis of four directions of backtrajectories from 1 August to 15 September, 2008. The bars show the standard deivations of SO_2 concentrations.

3.2 Case studies of SO_2 spatial distribution

3.2.1 Southeastern area: routes 1 and 2

Figure 5a and b overlay the SO_2 concentrations measured by the mobile laboratory and the wind field generated with the WRF model on 20 August and 4 September. The prevailing winds were from the SE and SSE with speeds of $1.2\pm0.2\,m\,s^{-1}$ and $3.6\pm1.2\,m\,s^{-1}$, respectively. The average mixing boundary layer height was 1027±232 m on 20 August and 1223±48 m on 4 September (Fig. S4). On both days, SO_2 concentrations had apparent horizontal gradients, increasing from urban to rural areas (Fig. 6) and clearly reflecting the transport patterns of SO_2 from the source regions in the southern area. Notably, the temporal variations of SO_2 emissions may be convoluted with the spatial variability due to the driving speed of the mobile. However, since the wind speeds in both the measuring days were not fast, assuming that the SO_2 emissions during measurement period were stable and the air masses were large enough, this influence on the SO_2 distributions would be expected low. Figure 5a, b show that high SO_2 concentrations were observed for approximately 30 km along the 5th and 6th Ring Roads, implying large-scale air mass transport. The mean value of SO_2 on 4 September was 14.9±3.2 ppb, twice as high as the 6.8±2.1 ppb observed on 20 August

3.2.2 Southeastern area: routes 3 and 4 between Beijing and Tianjin

Measurements were also conducted on a larger scale on routes 3 and 4 from Beijing to Tianjin on 3 and 11 September. The wind speeds on both days were similar: $2.38\pm0.27\,m\,s^{-1}$ and $2.04\pm0.15\,m\,s^{-1}$, respectively. The boundary layer was high on 3 September (1220±150 m) and relatively low on 11 September (833±267 m). The low boundary layer on 11 September is mainly due to the strong inversion layer and the weak wind near the surface. Figure 5c shows consistent decreasing trends of SO_2 concentration from Tianjin to Beijing on 3 September, under southeasterly prevailing winds, indicating the regional transport of SO_2 from relatively distant sources. The average SO_2 concentrations along route 3 were modestly high, about 23 ppb. The maximum SO_2 concentration of over 40 ppb was observed in the industrial centers of Tianjin, Tanggu, and Hangu (Fig. 6). In contrast, SO_2 concentrations had a very different distribution on 11 September (Fig. 5d), when the northwesterly wind dominated. The SO_2 concentrations were low, with an average concentration of around 5 ppb along route 4 (Fig. 6), while SO_2 concentrations in Beijing and Tianjin were relatively high. This suggests that SO_2 in the cities came mainly from local SO_2 emission sources.

3.2.3 Southwestern area: route 5 surrounding Beijing

We previously reported high concentrations of SO_2 and other pollutants in the Shijingshan district and along Jingkai Highway on 6 August 2008 and suggested this pollution was possibly from both local emission and regional transport (Wang et al., 2009a), but we had no further evidence to support this suggestion. In the particle number size distributions (Fig. 7c), we found bimodality with a remarkably high peak of ultrafine particle number concentrations in the 14.9–100 nm range and a smaller peak in the range larger than 100 nm, along Jingshi Highway. A similar observation was found in the Shijingshan district, but with lower particle number concentration peaks. Local emissions sources such as traffic exhaust, industrial emission, and biomass burning were identified as the major contributors to the particle number concentrations in the small particle size range, while the larger size particles were "aged," having formed during regional transport. Thus, we believe that the increase in SO_2 recorded along Jingshi Highway (Fig. 7b) was caused by both local emissions and regional transport.

To further investigate the high SO_2 concentrations in the Shijingshan district, we used the high-resolution wind field from the WRF simulation. As shown in Fig. 7a, on 6 August the observation along Jingshi Highway was dominated by winds flowing toward the northeast area, with the Shijingshan district located precisely downwind. Pollutants dispersed along the downwind direction from Jingshi Highway,

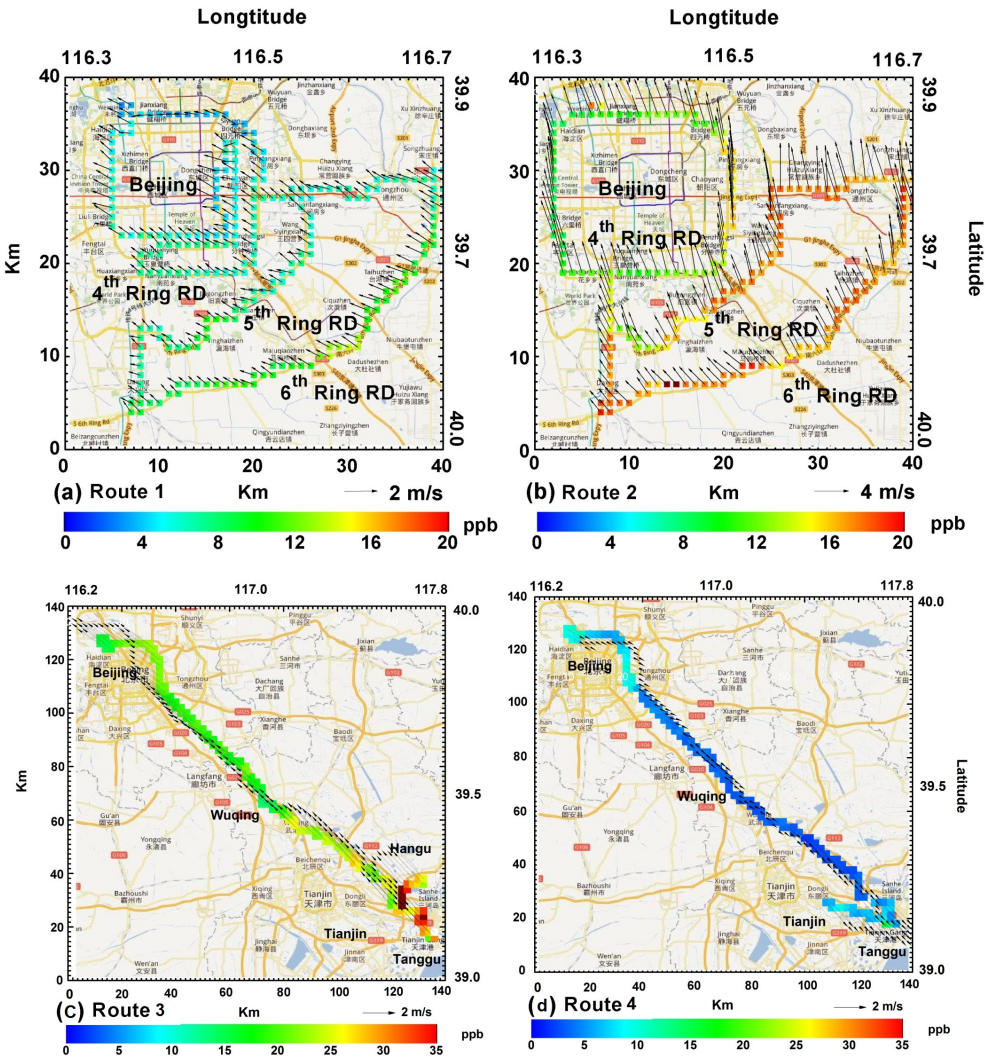

Fig. 5. The spatial distributions of SO_2 concentrations and wind field by WRF with 1×1 km grids resolution in southeastern areas of Beijing on **(a)** 20 August and **(b)** 4 September 2008, and 2×2 km grids from Beijing to Tianjin on **(c)** 3 September and **(d)** 11 September 2008.

leading to a high peak in SO_2 concentration across the Shijingshan district (see Fig. 7b dashed boxes).

The first peak of SO_2 at Shijingshan section shows clearly an overlap of the local emission and regional transported SO_2. We used a simple spline interpolation to separate the SO_2 from local emission (shaded area of the first Shijianshan peak in Fig. 7b) and regional transport (underneath the red dots of the first Shijianshan peak in Fig. 7b). The SO_2 from local emission was estimated by extracting the regional transport of SO_2 from the measured SO_2 concentration. With this, we estimated the local emission from Jingshi Highway to the Shijingshan district represented 16 % of the measured SO_2 concentrations.

3.3 Impacts of potential determinants on the measurements

The mean level of SO_2 differed significantly in the southeast of the 4th to 6th Ring Roads between 20 August and 6 September, although the wind field was similar in these days. Several factors might have influenced the variation of SO_2 over different days, e.g. variability of the strength of emission sources, prevailing transport directions, and dilutions over time. Figure 8 shows the spatial distributions of SO_2 emission during the emission control and non-control period and their emission differences. The emission inventories of Beijing, Tianjin and Hebei provinces were provided by Beijing Environmental Protection Bureau (EPB); for the other regions, we applied East Asia TRACE-P to extend surface sources and INTEX-B for the power plants' emission (Streets et al., 2003; Zhang et al., 2009). Emissions reduction

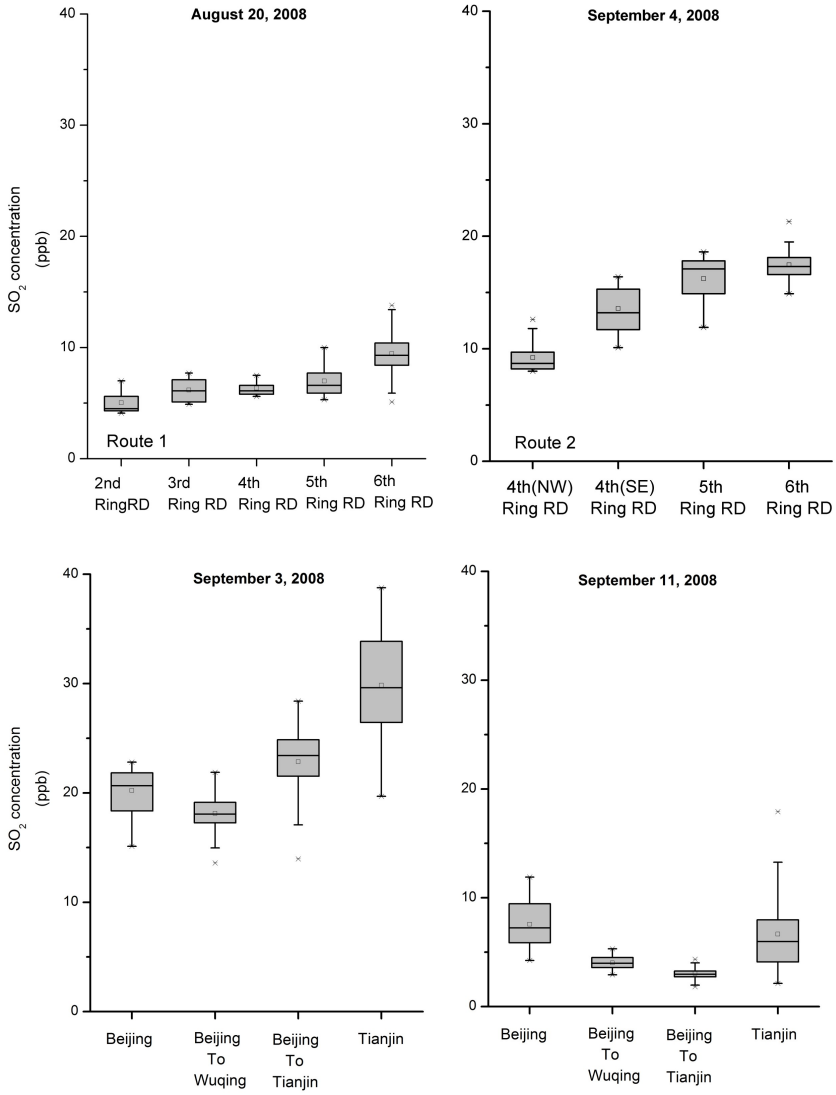

Fig. 6. Boxplots of the SO_2 concentrations on the ring roads in southeast of Beijing during the measurement periods. The small block indicates the mean value and the upper, middle and bottom layers of the box show the 75, 50, 25th percentiles of the dataset. The bars are determined by the 5 and 95th percentiles of the dataset and '×' show the maximum and minimum values respectively.

Table 3. SO_2 import fluxes and local emission derived from mobile laboratory in different routes surrounding Beijing.

	SO_2 flux ($kg\,s^{-1}$)				
	4th Ring RD SE	5th Ring RD SE	6th Ring RD SE	5th Ring RD SW	Shijingshan
6 Aug 2008				1.6	0.1
20 Aug 2008	0.2	0.4	1.6		
4 Sep 2008	2.1	4.0	4.6		

control inventory during the Olympics was mainly based on Beijing EPB emission control policies, taking into account of the desulfurization processes for industries in Beijing and neighboring regions. A high rate of SO_2 emissions was generated in the southern area of Beijing and in the Tianjin area which were in agreement with our measurements in Shijingshan area as well as the region southeast to Tianjin. In addition, high emissions were also observed, as expected, in

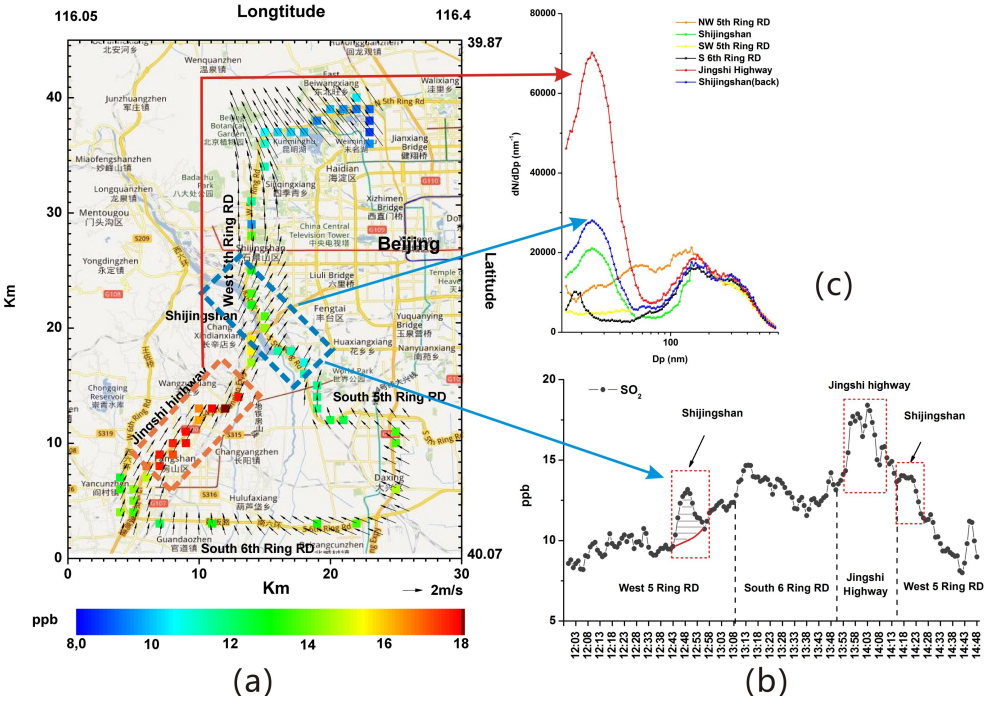

Fig. 7. **(a)** SO_2 spatial distributions and wind field by WRF with $1\times1\,km^2$ grids resolution in southwestern areas of Beijing on 6 August 2008. The dashed areas on the left and middle of the figure represent Jingshi Highway and Shijingshan district where high peak values were observed; **(b)** time series of SO_2 variations on 6 August, where the red plots and the black shades show the regional background and local emission of SO_2 across the 5th Ring Road. **(c)** SMPS particle size distributions measured in seperated areas of the route on 6 August. The red and blue arrows display the Jingshi Highway and Shijingshan districts in **(a)** corresponding to the SO_2 peak values in **(b)** and the particle size distributions in **(c)**.

Table 4. The annual SO_2 emission rates in provinces surrounding Beijing from Beijing EPB and INTEX-B 2006 inventory and the extrapolated SO_2 annual flux in our study.

Province	SO_2 non-control period ($Gg\,yr^{-1}$)	SO_2 control period ($Gg\,yr^{-1}$)	Sources
Beijing	200	70	Beijing EPB, 2008
Tianjin	414	324	Beijing EPB, 2008
Hebei	1705	1316	Beijing EPB, 2008
Shandong	3145	3145	INTEX-B 2006
Shanxi	2995	2965	INTEX-B 2006
Beijing 4th Ring RD	65.3	6.6	This study
Beijing 5th Ring RD	126.7	12.9	This study
Beijing 6th Ring RD	146.3	49.2	This study

the north of Shandong, south of Hebei and east of Shanxi provinces, where many industries are located. In constrast, numerous emissions were partially reduced or completely ceased during the control period. It was apparent that emissions in Beijing and Tianjin were largely and efficiently reduced with a decrease of 2 to 78 $Gg\,yr^{-1}$. In addition, most of the area in the south, in Hebei province and in the north, in Shandong province was also widely controlled. Summing up emissions by regions (table 4), Beijing had the highest reduction rate and lowest emissions of SO_2, followed by Tianjin, Hebei, Shanxi and Shandong provinces. Emissions in Beijing decreased from 200 to 70 $Gg\,yr^{-1}$ because of the strict and most widely-applied control measures restricting industrial activity and traffic emissions. It was worth noting that emissions in Shandong province under control and non-control periods were not different, which does not necessarily indicate no effects of control measures but could reflect a balance between decrease of SO_2 in the north and increase

of SO_2 in the south of Shandong. Overall, SO_2 emissions were effectively controlled in the south and southeast areas surrounding Beijing, implying spatial variations of emission patterns which were attributed to the concentration differences between 20 August and 4 September.

To investigate the transport sources, the 48 h backward trajectory of the air mass on 20 August retraced from the Tianjin area and dispersed around the suburban and urban area between Beijing and Tianjin (Fig. 9a). As shown in Fig. 8 and Table 4, the emissions from Tianjin city were much lower than the emissions from the other provinces, hence low SO_2 concentrations were to be expected. On 4 September (Fig. 9b), however, the 48 h backward trajectory originated from the mid-eastern mainland of China, traveling northward across Hebei, Henan, and even Shandong provinces. These areas contain numerous thriving industrialized cities where anthropogenic pollutants, especially SO_2, are generated (Streets et al., 2007). Liu et al. (2010) reported that the neighboring provinces around Beijing, such as Shandong, Hebei and Shanxi provinces, contribute a large amount of the total SO_2 emissions of China. SO_2 emission rate in this area was more than tenfold that of Tianjin. Air masses flowing across these regions usually pick up heavy pollutants downwind, leading to high concentrations of SO_2.

SO_2 concentration variations may also be influenced by the variability in dilutions in processes of chemical transformations and depositions. The reactions and depositions for SO_2 during the transport were different under various meteorological conditions. Low wind speed and relatively high humidity on 20 August was favorable for the transformations of SO_2 to sulfate and shortening of the life time in distance travelled. On the contrary, strong wind on 4 September likely decreased the deposition over time. Besides, since the boundary layer on 20 August was not fully developed during the morning sampling period, upwind SO_2 sources from power plants may not have fully mixed down to the surface layer, the detrainment of SO_2 into the free troposphere of elevated sources from power plant stacks may have led to potential bias of SO_2 detection by the measurements.

3.4 Estimate of SO_2 influx to Beijing

Table 3 lists the flux of SO_2 through the Ring Roads on 6 and 20 August and 4 September calculated with Eq. (1), assuming homogenous wind fields. The SO_2 flux on the 5th Ring Road on 6 August was determined as 1.6 kg s^{-1}, with 2.9 m s^{-1} wind speed and 1140±233 m boundary layer height. The flux of local emissions on Jingshi Highway was assessed by calculating the downwind SO_2 traverse at the southwestern 5th Ring Road in the Shijingshan district; and yielded a SO_2 flux of 0.1 kg s^{-1}. The flux of SO_2 increased from the 4th to 6th Ring Roads, from 0.2 to 1.6 kg s^{-1} on 20 August, and from 2.1 to 4.6 kg s^{-1} on 4 September. The large difference between the estimated fluxes of SO_2 could be explained by the differences in SO_2 concentrations and

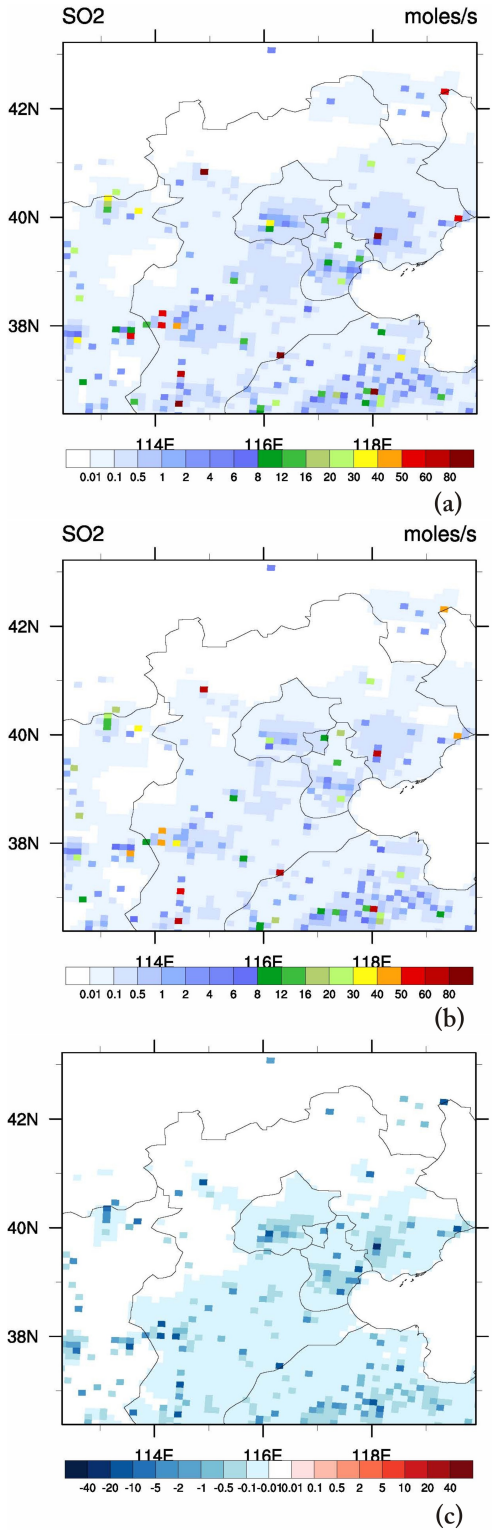

Fig. 8. Spatial distributions of anthropogenic SO_2 in and around Beijing with horizontal resolution of 12 by 12 km^2 during the emission **(a)** non-control and **(b)** control periods and **(c)** their differences in between.

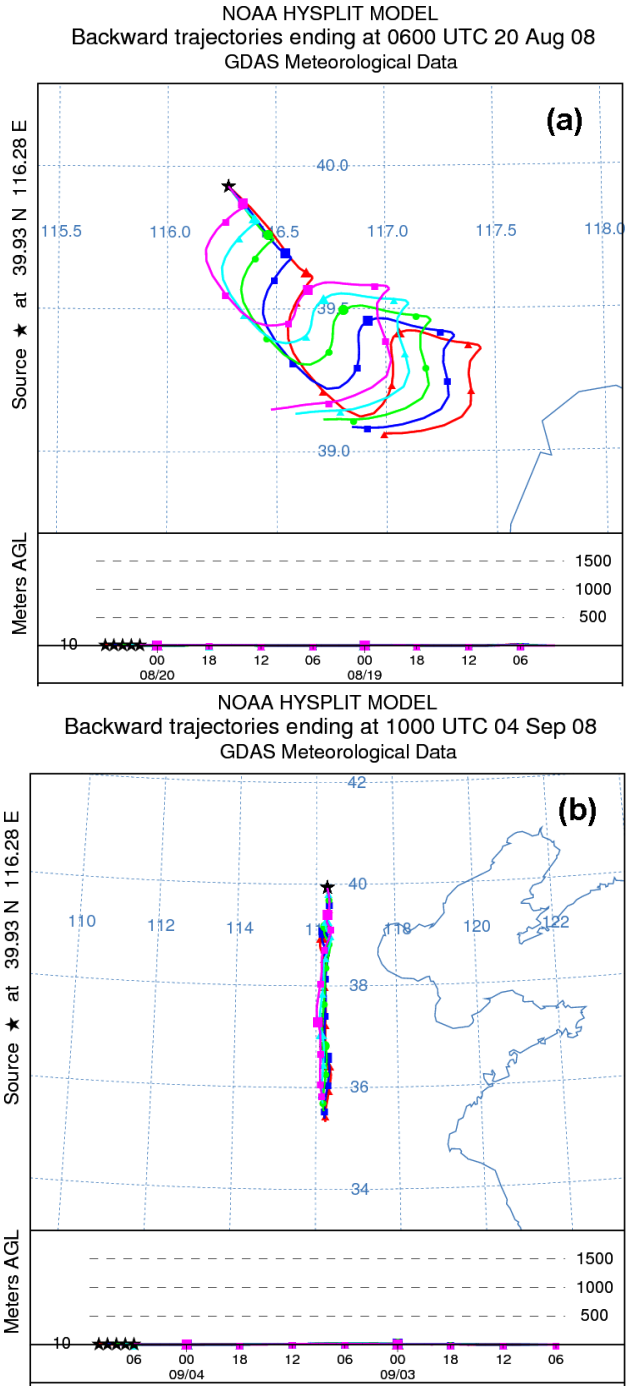

Fig. 9. 48 h backward trajectories for Beijing on 20 August **(a)** and 4 September **(b)**, 2008 at a height of 10 m. The multiple tracks (1 track per hour) in figures show the sources during the measurement periods.

meteorological conditions e.g. wind speed and direction between those sampling days. The SO_2 concentration variations might be due to abovementioned factors: (1) variations of SO_2 spatial patterns during the control and non-control periods; (2) variations of source directions in various emission strength areas, and (3) variations of dilutions over sampling days.

The magnitude of derived influxes through the 6th Ring Rd is roughly equivalent to a reported single large power plant (Wang et al., 2006) or an industrial complex (Rivera et al., 2009) with emission rates of 2.1 kg s^{-1} and 4.4 kg s^{-1}, respectively, regardless of the transformation and deposition processes during the transport. Table 4 compares the emission inventory from Beijing EPB (Wu et al., 2010) and INTEX-B with the calculated SO_2 fluxes measured on 20 August and 4 September at the Ring Roads. The calculated SO_2 influxes were extrapolated to the annual SO_2 influxes by assuming a constant emission rate over a year. It is shown that in the non control period the annual influxes of SO_2 through the southeast of the 6th Ring Road into Beijing could be as high as 146.3 Gg yr^{-1}, which is 73 % of the 200 Gg yr^{-1} annual SO_2 emission in Beijing; during the control period, the extrapolated annual influxes of SO_2 through the southeast of the 6th Ring Road has been reduced to 49.2 Gg yr^{-1}, but is still 70 % of the extrapolated 70 Gg yr^{-1} of annual SO_2 emission in Beijing. These suggest that within the 6th ring in Beijing the transport of SO_2 contributed greatly to the SO_2 concentration. Direct comparison between measured data with emission sources seems difficult. Here we applied the SOR index (molar ratio of particulate sulfate to total SO_4^{2-}+SO_2) for the estimation of SO_2 from regional sources, which has been measured in rural Beijing during the summer time in 2006 (Guo et al., 2010). After the transformation, the total influxes of SO_x in Beijing were estimated to be from 287 to 431 Gg yr^{-1} in the control period, which was much closer to the emission levels observed in Tianjin. Similarly, estimated SOx was 853 to 1280 Gg yr^{-1} in the non-control period, which was also comparable to the emissions from Hebei province. However, since all the emissions were calculated regardless of the life time and deposition process, and the derived flux was time-dependent and was not representative of the average emissions in years, the yielding emission rates may be underestimated. Apparently, high uncertainties are associated with the SO_2 flux measurements and this extrapolation, but our results yield a relative importance of the SO_2 transport similar to that previously reported model estimation of a heavy pollution episode (An et al., 2007).

3.5 Uncertainty

Uncertainty in estimates of the SO_2 flux in this study may come from the sampling strategy, imperfect knowledge in both horizontal and vertical distributions of wind profiles, the height of boundary layers, and the time interval across the plume (Wang et al., 2008). In our study, sampling error due to local turbulences (e.g. street canyon) was minor because most of the routes were located between urban and rural areas which were far away from high buildings. Influences by

hotspots from vehicles nearby were intentionally avoided by keeping distance (>10 m) away from vehicles in front. As for the wind field, the horizontal differences in wind speed and direction found by the WRF model were 19 % and 7.5 % compared to the station monitoring data. In addition, using surface wind data for vertical wind profile due to lack of observational information might have underestimated the effectiveness of wind speed for the SO_2 influx. However, given that most of the emission sources were located on the surface (except for e.g. power plants), the introduced underestimation is expected to be not so significant (Ibrahim et al., 2010). Regarding SO_2 emissions from high stacks, e.g. power plants, it is noteworthy that despite the critical effect of updrafts exchanged in the unstable free atmosphere layer (on 20 August), the estimation error was fairly small considering the long range transport in our cases (Krautstrunk et al., 2000). Zhu et al. (2010) observed a homogeneous vertical distribution of SO_2 in daytime in Beijing with DOAS measurements, which suggests our assumption of homogeneous vertical distribution of SO_2 is justified. Since observational retrieved extinction coefficients from lidar were not available for every measured period due to meteorological conditions, and single site comparison with the model lacked representations of spatial variation, quantitative errors for the estimated PBL cannot be computed. Qualitatively, the predictive error was about one third. Errors from temporal variations in wind field were relatively low given the smaller spatial scale of the wind fluctuations with respect to the spatial extent of areas of enhanced SO_2 concentrations (Ibrahim et al., 2010). A sensitivity analysis indicated approximate 12 % deviations of SO_2 fluxes using wind field in individual hours instead of averages. Therefore, the overall error is approximately 31 %.

4 Conclusions

We used a mobile laboratory to identify and assess the transport processes and emission sources of SO_2 surrounding Beijing in combination with the wind field distribution. The measurements were conducted as a part of the CAREBeijing-2008 campaign from August to September 2008, and covered the southeast and southwest areas surrounding Beijing.

Continuous measurements at the PKU urban station and the YuFa and YongLeDian rural stations were performed before, during, and after the comprehensive control period. Three potential pollution periods were identified, with short backwards trajectories from the south and southeast areas outside Beijing.

Mobile monitoring was conducted to investigate the regional transport of SO_2 from the southern mainland of China. We designed three routes. The route along the southeast of the Ring Roads reflected the wide scope of the polluted plumes, while the "straight line" between Beijing and Tianjin further supported the regional transport of SO_2 over long distances. We also noticed that the plumes from the center of mainland China usually picked up pollutants along the way, leading to high concentrations on 4 September compared to those on 20 August. On 6 August, regional transport from southeast areas as well as local emissions on Jingshi Highway and their dispersion over the downwind district of Shijingshan were identified and demonstrated by WRF simulations and particle size-distribution measurements.

Using a simple method assuming constant wind speed and directions within 1 h and homogeneous vertical profiles of the well-mixed boundary layer, we found that the flux of SO_2 transported to Beijing was high on 4 September and low on 20 August. From the 4th to the 6th Ring Roads, the SO_2 flux ranged from 2.1 to 4.6 on 4 September and 0.2 to 1.6 $kg\,s^{-1}$ on 20 August. The difference in influxes between days can be explained by the variability in emissions in areas due to the control policy, the transport directions and the dilution processes on the way. Influx from the southwest on 6 August across the 5th Ring Road was 1.6 $kg\,s^{-1}$. Local emission on Jingshi Highway was roughly 0.1 $kg\,s^{-1}$. In summary, mobile monitoring is a useful approach to evaluate temporal and spatial variations in SO_2 transport processes. The uncertainty of the SO_2 flux is estimated to approximately 31 %.

Supplement related to this article is available online at: http://www.atmos-chem-phys.net/11/11631/2011/ acp-11-11631-2011-supplement.pdf.

Acknowledgements. This study was supported by the Beijing Environmental Protection Bureau (OITC-G08026056). We would like to thank TSI Inc. for their assistance on SMPS instrument support. Special thanks also to the Chinese Meteorological Administration for meteorological data support. We also acknowledge Xiao Tang, Weili Lin and V. C. Lenters for providing precious advice on back trajectory models and data analysis. Finally, we thank NOAA for the data support of the back trajectory model.

Edited by: D. Parrish

References

An, X., Zhu, T., Wang, Z., Li, C., and Wang, Y.: A modeling analysis of a heavy air pollution episode occurred in Beijing, Atmos. Chem. Phys., 7, 3103–3114, doi:10.5194/acp-7-3103-2007, 2007.

Beijing Statistical Yearbook: China Statistics Press, Beijing, China, chapter 4.2, 2009.

Beryrich, F., Grafe, H., Kuchler, W., Lindemann, C., and Schaller, E.: An obervational study of sulphur dioxide transport across the erzgebirge mountains, Atmos. Environ., 32, 1027–1038, 1998.

Brunekreef, B. and Holgate, S. T.: Air pollution and health, Lancet, 360, 1233–1242, 2002.

Bukowiecki, N., Dommen, J., Prevot, A. S. H., Richter, R., Weingartner, E., and Baltensperger, U.: A mobile pollutant measurement laboratory-measuring gas phase and aerosol ambient concentrations with high spatial and temporal resolution, Atmos. Environ., 36, 5569–5579, 2002.

Canagaratna, M. R., Jayne, J. T., Ghertner, D. A., Herndon, S., Shi, Q., Jimenez, J. L., Silva, P. J., Williams, P., Lanni, T., Drewnick, F., Demerjian, K., Kolb, C. E., and Worsnop, D. R.: Chase Studies of Particulate Emissions from in-use New York City Vehicles, Aerosol Sci. Technol., 38, 2004,

Ding, A. J., Wang, T., Xue, L. K., Gao, J., Stohl, A., Lei, H. C., Jin, D. Z., Ren, Y., Wang, X. Z., Wei, X. L., Qi, Y. B., Liu, J., and Zhang, X. Q.: Transport of north china air pollution by midlatitude cyclones: Case study of aircraft measurements in summer 2007, J. Geophys. Res.-Atmos., 114, D11399, doi:10.1029/2009jd012339, 2009.

Draxler, R. R. and Rolph, G. D.: Hysplit (hybrid single-particle lagrangian integrated trajectory) model access via noaa arl ready website http://www.Arl.Noaa.Gov/ready/hysplit4.html, NOAA Air Resources Laboratory, 2003.

Guo, S., Hu, M., Wang, Z. B., Slanina, J., and Zhao, Y. L.: Size-resolved aerosol water-soluble ionic compositions in the summer of beijing: Implication of regional secondary formation, Atmos. Chem. Phys., 10, 947–959, doi:10.5194/acp-10-947-2010, 2010.

Hebei Statistical Yearbook, China Statistics Press, Beijing, China, Sect. 9.2, 2009.

Herndon, S. C., Jayne, J. T., Zahniser, M. S., Worsnop, D. R., Knighton, B., Alwine, E., Lamb, B. K., Zavala, M., Nelson, D. D., McManus, J. B., Shorter, J. H., Canagaratna, M. R., Onasch, T. B., and Kolb, C. E: Characterization of urban pollutant emission fluxes and ambient concentration distributions using a mobile laboratory with rapid response instrumentation, Faraday Discuss., 130, 327–339, 2005.

Ibrahim, O., Shaiganfar, R., Sinreich, R., Stein, T., Platt, U., and Wagner, T.: Car MAX-DOAS measurements around entire cities: quantification of NO_x emissions from the cities of Mannheim and Ludwigshafen (Germany), Atmos. Meas. Tech., 3, 709–721, doi:10.5194/amt-10-709-2010, 2010.

Johansson, M., Galle, B., Yu, T., Tang, L., Chen, D., Li, H. J., Li, J. X., and Zhang, Y.: Quantification of total emission of air pollutants from beijing using mobile mini-doas, Atmos. Environ., 42, 6926–6933, 2008.

Johansson, M., Rivera, C., de Foy, B., Lei, W., Song, J., Zhang, Y., Galle, B., and Molina, L.: Mobile mini-doas measurement of the outflow of NO_2 and HCHO from mexico city, Atmos. Chem. Phys., 9, 5647–5653, doi:10.5194/acp-9-5647-2009, 2009.

Krautstrunk, M., Neumann-Hauf, G., Schlager, H., Klemm, O., Beyrich, F., Corsmeier, U., Kalthoff, N., and Kotzain, M.: An experimental study on the planetary boundary layer transport of air pollutants over East Germany, Atmos. Environ., 34, 1247–1266, 2000.

Li, A., Xie, P. H., Liu, W. Q., Liu, J. G., Dou, K.: Studies on the determination of the flux of gaseous pollutant from an area by passive differential optical absorption spectroscopy, (in Chinese), Spectrosc. Spect. Analys., 29, 28–32, 2009.

Li, C., Krotkov, N. A., Dickerson, R. R., Li, Z. Q., Yang, K., and Chin, M.: Transport and evolution of a pollution plume from Northern China: A satellite-based case study, J. Geophys. Res.-Atmos., 115, D00K03, doi:10.1029/2009jd012245, 2010.

Liu, J., Zhang, X. L., Xu, X. F., and Xu, H. H.: Comparison analysis of variation characteristics of SO_2, NO_x, O_3 and $PM_{2.5}$ between rural and urban areas, Beijing, Environ. Sci., 29, 1059-1065, 2008.

Liu, Z., Street, D. G., Zhang, Q., Wang, S., Carmichael, G. R., Cheng, Y. F., Wei, C., Chin, M., Diehl, T., and Tan, Q.: Sulfur dioxide emissions in China and sulfur trends in East Asia since 2000, Atmos. Chem. Phys., 10, 6311–6331, doi:10.5194/acp-10-6311-2010, 2010.

Matsui, H., Koike, M., Kondo, Y., Takegawa, N., Kita, K., Miyazaki, Y., Hu, M., Chang, S. Y., Blake, D. R., Fast, J. D., Zaveri, R. A., Streets, D. G., Zhang, Q., and Zhu, T.: Spatial and temporal variations of aerosols around beijing in summer 2006: Model evaluation and source apportionment, J. Geophys. Res.-Atmos., 114, D00G13, doi:10.1029/2008JD010906, 2009.

Ma, J. Z., Chen, Y., Wang, W., Yan, P., Liu, H. J., Yang, S. Y., Hu, Z. J., and Lelieveld, J.: Strong air pollution causes widespread haze-clouds over China, J. Geophys. Res.-Atmos., 115, D18204, doi:10.1029/2009JD013065, 2010.

Matvev, V., Dayan, U., Tass, I., and Peleg, M.: Atmospheric sulfur flux rates to and from israel, The Science of the Total Environment 291, 143-154, 2002.

Ohara, T., Akimoto, H., Kurokawa, J., Horii, N., Yamaji, K., Yan, X., and Hayasaka, T.: An asian emission inventory of anthropogenic emission sources for the period 1980–2020, Atmos. Chem. Phys., 7, 4419–4444, doi:10.5194/acp-7-4419-2007, 2007.

Qin, M., Xie, P. H., Wu, D. X., Xu, J., Si, F. Q., Wang, M. H., Dou, K., Zhang, Y., Xiao, X., Liu, W. S., Liu, S. S., Wang, F. P., Fang, W., Liu, J. G., and Liu, W. Q.: Investigation of variation characteristics and levels of SO_2-NO_2-O_3 and pm10 in Beijing during 2008 Olympic Games, J. Atmos. Environ. Opt., 4, 329–340, 2009.

Ramanathan, V. and Crutzen, P. J.: New directions: Atmospheric brown "Clouds", Atmos. Environ., 37, 4033–4035, 2003.

Rivera, C., Sosa, G., Wohrnschimmel, H., de Foy, B., Johansson, M., and Galle, B.: Tula industrial complex (mexico) emissions of SO_2 and NO_2 during the MCMA 2006 field campaign using a mobile mini-doas system, Atmos. Chem. Phys., 9, 6351–6361, doi:10.5194/acp-9-6351-2009, 2009.

Shaiganfar, R., Beirle, S., Sharma, M., Chauhan, A., Singh, R. P., and Wagner, T.: Estimation of NO_x emissions from Delhi using Car MAX-DOAS observations and comparison with OMI satellite data, Atmos. Chem. Phys., 11, 10871–10887, doi:10.5194/acp-11-10871-2011, 2011.

Shandong Statistical Yearbook, China Statistics Press, Beijing, China, chapter 6-2, 2009.

Shanxi Statistical Yearbook, China Statistics Press. Beijing, China, chapter 4.10, 2009.

Streets, D., Bond, T., Carmichael, G., Fernandes, S. D., Fu, Q., He, D., Klimont, Z., Nelson, S. M., Tsai, N. Y., Wang, M. Q., Woo, J. H., and Yarber, K. F.: An inventory of gaseous and primary aerosol emission in Asia in the year 2000, J. Geophys. Res.-Atmos., 108, 8809, doi:10.1029/2002JD003093, 2003.

Streets, D. G., Fu, J. S., Jang, C. J., Hao, J. M., He, K. B., Tang, X. Y., Zhang, Y. H., Wang, Z. F., Li, Z. P., Zhang, Q., Wang, L. T., Wang, B. Y., and Yu, C.: Air quality during the 2008 beijing olympic games, Atmos. Environ., 41, 480–492, 2007.

Sun, Y., Wang, Y. S., and Zhang, C. C.: Measurement of the vertical profile of atmospheric SO_2 during the heating period in Beijing on days of high air pollution, Atmos. Environ., 43, 468–472, 2009.

Sun, Y. L., Zhuang, G. S., Wang, Y., and Han, L. H.: The airborne particulate pollution in beijing-concentration, composition, dis-

tribution and sources, Atmos. Environ., 38, 5991–6004, 2004.

Tianjin Statistical Yearbook, China Statistics Press. Beijing, China, chapter 5.1, 2009.

Wang, M., Zhu, T., Zheng, J., Zhang, R. Y., Zhang, S. Q., Xie, X. X., Han, Y. Q., and Li, Y.: Use of a mobile laboratory to evaluate changes in on-road air pollutants during the beijing 2008 summer olympics, Atmos. Chem. Phys., 9, 8247–8263, 2009a, http://www.atmos-chem-phys.net/9/8247/2009/.

Wang, P., Richter, A., Bruns, M., Burrows, J. P., Scheele, R., Junkermann, W., Heue, K. P., Wagner, T., Platt, U., and Pundt, I.: Airborne multi-axis DOAS measurements of tropospheric SO_2 plumes in the PO-valley, Italy, Atmos. Chem. Phys., 6, 329–338, doi:10.5194/acp-6-329-2006, 2006.

Wang, W., Ren, L. H., Zhang, Y. H., Chen, J. H., Liu, H. J., Bao, L. F., Fan, S. J., and Tang, D. G.: Aircraft measurements of gaseous pollutants and particulate matter over pearl river delta in china, Atmos. Environ., 42, 6187–6202, 2008.

Wang, Y., Hao, J., McElroy, M. B., Munger, J. W., Ma, H., Chen, D., and Nielsen, C. P.: Ozone air quality during the 2008 beijing olympics: Effectiveness of emission restrictions, Atmos. Chem. Phys., 9, 5237–5251, doi:10.5194/acp-9-5237-2009, 2009b.

Weijers, E. P., Khlystov, A. Y., Kos, G. P. A., and Erisman, J. W.: Variability of particulate matter concentrations along roads and motorways determined by a moving measurement unit, Atmos. Environ., 38, 2993–3002, 2004.

White, W. H., Anderson, J. A., Blumenthal, D. L., Husar, R. B., Gillani, N. V., Husar, J. D., and Wilson, W. E.: Formation and transport of secondary air pollutants: ozone and aerosols in the St. Louis urban plume, Science, 194, 187–189, 1976.

Wu, Q. Z.: Developing and applying multiple air quality prediction modeling system for Beijing, dipl. thesis, 76–78, 2010.

Xu, X. D., Zhou, L., and Zhou, X. J.: Urban environment region influenced by surrounding sources during serious atmospheric pollution process, Sci. China D Earth Sci., 34, 958–966, 2004.

Xu, X. P., Wang, L. H., and Niu, T. H.: Air pollution and its health effects in beijing, Ecosyst. Health, 4, 199–209, 1998.

Zhang, M. G., Uno, I., Yoshida, Y., Xu, Y. F., Wang, Z. F., Akimoto, H., Bates, T., Quinn, T., Bandy, A., and Blomquist, B.: Transport and transformation of sulfur compounds over east asia during the trace-p and ace-asia campaigns, Atmos. Environ., 38, 6947–6959, 2004a.

Zhang, Q., Streets, D. G., Carmichael, G. R., He, K. B., Huo, H., Kannari, A., Klimont, Z., Park, I. S., Reddy, S., Fu, J. S., Chen, D., Duan, L., Lei, Y., Wang, L. T., and Yao, Z. L.: Asian emissions in 2006 for the NASA INTEX-B mission, Atmos. Chem. Phys., 9, 5131–5153, doi:10.5194/acp-9-5131-2009, 2009.

Zhang, Z. G., Gao, Q. X., and Han, X. Q.: The study of pollutant transport between the cities in north china, Res. Environ. Sci., 17, 14–20, 2004b.

Zhu, Y. W., Liu, W. Q., Xie, P. H., Dou, K., Qin, M., and Si, F. Q.: Monitoring and analysis for vertical profiles of air pollutants in boundary layer of Beijing (in Chinese), Chinese J. Geophys., 53, 1278–1283, 2010.